Nanoscale

Accepted Manuscript

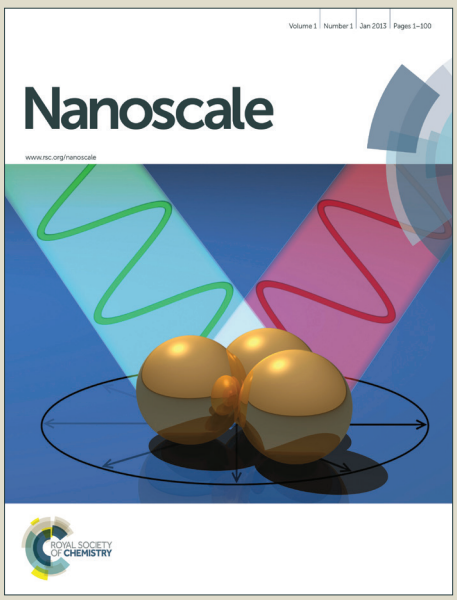

ROYAL SOCIETY OF CHEMISTRY

www.rsc.org/nanoscale

Nanoscale

RSC Publishing

PAPER

The Influence of Nanoscale Roughness and Substrate Chemistry on the Frictional Properties of Single and Few Layer Graphene

Cite this: DOI: 10.1039/xoxxoooooox

Jessica C. Spear,[a] James P. Custer[b] and James D. Batteas*[c]

Nanoscale carbon lubricants such as graphene, have garnered increased interest as protective surface coatings for devices, but its tribological properties have been shown to depend on its interactions with the underlying substrate surface and its degree of surface conformity. This conformity is especially of interest as real interfaces exhibit roughness on the order of ~ 10 nm that can dramatically impact the contact area between the graphene film and the substrate. To examine the combined effects of surface interaction strength and roughness on the frictional properties of graphene, a combination of Atomic Force Microscopy (AFM) and Raman microspectroscopy has been used to explore substrate interactions and the frictional properties of single and few-layer graphene as a coating on silica nanoparticle films, which yield surfaces that mimic the nanoscaled asperities found in realistic devices. The interactions between the graphene and the substrate have been controlled by comparing their binding to hydrophilic (silanol terminated) and hydrophobic (octadecyltrichlorosilane modified) silica surfaces. AFM measurements revealed that graphene only partially conforms to the rough surfaces, with decreasing conformity, as the number of layers increase. Under higher mechanical loading the graphene conformity could be reversibly increased, allowing for a local estimation of the out-of-plane bending modulus of the film. The frictional properties were also found to depend on the number of layers, with the largest friction observed on single layers, ultimately decreasing to that of bulk graphite. This trend however, was found to disappear, depending on the tip-sample contact area and interfacial shear strain of the graphene associated with its adhesion to the substrate.

Received ooth January 201X,
Accepted ooth January 201X

DOI: 10.1039/xoxxoooooox

www.rsc.org/

Since its discovery in 2004,[1] graphene has revolutionized a new field of study in two-dimensional nanomaterials. Although the structure of graphene is a simple honeycomb carbon lattice, it has unique electronic and mechanical properties including ballistic electron transport,[2] high thermal conductivity,[3] large in-plane elastic modulus[4] and a low coefficient of friction.[5-7] These diverse properties expand the field of applications for graphene to include composite materials,[8] energy transfer[9] and storage,[10] electronic[11] and mechanical devices,[12] and solid-state lubrication.[5-7, 13]

Utilizing graphene in real devices however can be limited by the variability of its electronic and mechanical properties, which strongly depend on the interfacial interaction with the underlying substrate.[14, 15] Due to its high out-of-plane flexibility, the morphology of graphene is largely dictated by the geometry of the substrate on which it is deposited, which influences the measured properties through changes in electronic structure, topological defects, and chemical doping effects.[16-21] For example, graphene grown by chemical vapor deposition (CVD) on a copper catalyst demonstrated improved quality (decreased defects) when a smooth, polished surface was used as compared to a rough one.[22] Subsequently, the electronic properties of graphene were greatly enhanced on the smoother surface with higher measured hole mobility being attributed to the reduction of carrier scattering.

The frictional properties of graphene have also been reported to have a dependence on the substrate morphology and interfacial adhesion. On thermally grown silicon oxide, exfoliated graphene exhibited a "puckering effect" and a significantly increased measured friction for single-layers as compared to multi-layers and bulk graphite. However, when exfoliated onto atomically flat mica, the "puckering effect" was suppressed due to increased adhesion at the graphene-mica interface.[13] Cho and co-workers further studied the effect of surface morphology on the friction and adhesion of graphene and found that when graphene was folded from the silica substrate, the surface corrugations were preserved.[23] This resulted in an enhanced friction on the graphene even when folded onto a flat substrate

[a]*Department of Chemistry, Texas A&M University, College Station, TX 77843, USA.*
[b]*NSF-REU student from the Department of Chemistry, Muhlenberg College, Allentown, PA18104, USA.*
[c]*Department of Chemistry and Materials Science and Engineering, Texas A&M University, College Station, TX 77843, USA. E-mail: batteas@chem.tamu.edu*

† Electronic Supplementary Information (ESI) available: Raman and AFM results of graphene on unfunctionalized and OTS functionalized SiO_2/Si(100) substrates. Infrared spectroscopic characterization of the OTS substrates. See DOI: 10.1039/b000000x/

due to the decreased contact with the surface and lowered interfacial adhesion. These findings imply that strong adhesion to the substrate as well as good conformity are required for optimal frictional properties on graphene and that even small atomic scale roughness can decrease the interfacial binding.

In real devices, the nanoscopic morphology of surfaces can further amplify the effects of substrate interactions and warrant significant study. To address the challenges of graphene's substrate mediated properties, a complete fundamental understanding of the various interfacial interactions is needed in order to control the morphology and thus the properties of graphene. Studying surfaces with nanoscale roughness would aid in achieving this goal and is of particular interest for using graphene as a protective coating for microelectromechanical system devices, which exhibit nanoscale surface roughness on the order of 10 nm.[24] The interaction between graphene and structured surfaces has been studied predominately theoretically and found to be quite complex, involving an energy balance between the surface geometry, chemistry, bending energy and lattice strain.[25-31] These factors are critical in determining the morphology of graphene on such surfaces and can lead to a range of configurations from fully conformed to lying flat over the surface,[32] which would also affect the frictional behavior. The work in this paper centers around investigating the morphology and tribological properties of graphene exfoliated onto hydrophilic and hydrophobic nanoparticle films with controlled nanoscale roughness, to examine the interfacial interactions and resulting frictional and mechanical properties of graphene on such roughened surfaces.

Materials and Methods

Sample Preparation

Substrates with controlled nanoscopic roughness were prepared from a modified procedure found in the literature[33, 34] by spin-coating 20 nm diameter silica nanoparticles (Ludox) onto clean Si(100) score cut wafers (Virginia Semiconductor). A nanoparticle concentration of 6 wt% in high purity H_2O (18.2 MΩ·cm, Barnstead), and spin-coating parameters (400 µL, 2000 rpm, 2 min) were used to yield a film thickness ~ 90 nm. The nanoparticle films were then annealed in a kiln at 500º C for 5 hrs and unfunctionalized surfaces were then treated with UV/ozone before graphene transfer onto the particulate film to yield hydrophilic surfaces. This optimized film thickness provided exceptional optical contrast for observing the locations of the deposited graphene sheets.

To create hydrophobic surfaces, the particle films were silane functionalized with octadecyltrichlorosilane (OTS). The samples were first cleaned and hydroxylated with a 4:1:1 (v/v/v) solution of high purity H_2O (18.2 MΩ·cm, Barnstead), concentrated NH_4OH, and H_2O_2 (30%) for ~15 min at 85ºC (*Caution: Piranha solution is highly corrosive and reacts violently with organic matter*). The samples were rinsed with nanopure water, ethanol and dried with streaming nitrogen. Substrates were functionalized by sonicating (90 min) in ~1 mM OTS (Gelest)/hexanes solution and stored overnight (12 – 24 hrs). They were then sonicated in tetrahydrofuran, dried with nitrogen and characterized with FTIR Spectroscopy before graphene transfer.

As transfer of graphene by the Scotch tape method[1] was found to be of limited utility on these rough surfaces, we utilized a modified transfer approach as described here. Water soluble tape (3M) was used to exfoliate HOPG (K-Tek Nanotechnology) and transfer the flakes to the sample substrates. The tape was then dissolved in warm high purity water (85º C) and rinsed with high purity water. The samples were then dried with streaming nitrogen and stored in a desiccator overnight. To create graphene, the water soluble tape was again used to cleave part of the graphite from the surface leaving behind small areas of single and multi-layer graphene.

Fourier Transform Infrared (FTIR) Spectroscopy

Sample spectra were recorded with a Thermo Nicolet 6700 FTIR equipped with a liquid nitrogen-cooled MCT (HgCdTe) detector and a Harrick Scientific horizontal reflection Ge-attenuated total reflection accessory (VariGATR, incidence angle 65º). A semispherical Ge crystal was used as the optical element. Spectra were collected with 128 scans at a resolution of 1 cm^{-1} for the backgrounds and OTS functionalized samples.

Raman Microspectroscopy

A commercially available confocal Raman microscope (WITec Alpha 300R, Germany) was used for locating and characterizing single and multi-layer graphene regions under ambient conditions (20-25 ºC). The microscope was equipped with an Acton triple grating spectrometer interfaced with an Andor Peltier cooled (-65 ºC) CCD detector and a 488 nm Ar ion laser with a laser spot size of *ca.* 300 nm focused with a Nikon high numerical aperture objective (100x, 0.9 NA). The spectral resolution used was ~ 3 cm^{-1}. The laser power for all measurements was maintained below 1.5 mW.

Atomic Force Microscopy

Samples were imaged by AFM (Agilent 5500) with silicon tips (Mikromasch CSC37 for contact mode and Aspire CT170R for tapping-mode) under ambient conditions (45% - 55% RH and 20 ºC -25 ºC). The contact mode tips had force constants ranging from 0.1 – 0.8 N/m, depending on lever, and the spring constants were independently determined for each with the Sader method.[35] Tapping-mode tips had resonance frequencies in the range of 150 kHz – 210 kHz. Tip radii were determined experimentally from the blind tip reconstruction feature using Scanning Probe Image Processing (SPIP) Software (Image Metrology, Denmark). All images and roughness calculations were also processed with SPIP. Friction and roughness measurements were taken with a normal load of 5 nN on individual graphene layers. Raw friction data was analyzed by averaging the total lateral signal for each layer using the same tip and measuring all layers *in situ* on each sample for comparison.

Results and Discussion

As we have previously reported,[36] silica nanoparticles may be fused to silicon wafers to create surfaces with controlled nanoscale roughness, tunable by particle size, which allows for the formation of surfaces that mimic the nanoscale surface asperities often found in real devices[24] but with uniform roughness. Here we have prepared films consisting of 20 nm in diameter silica particles. The deposition of graphene on these rough surfaces was found to be difficult through normal mechanical exfoliation methods due to the stiffness of the graphite flakes and decreased contact area to the substrate.

To increase the transfer yield, water soluble tape was used to first deposit large (millimeter size) graphite flakes which were then partially re-cleaved from the surface, leaving thinner flakes with regions of single and few-layer graphene on the surface. Regions of the sample containing graphene layers were located

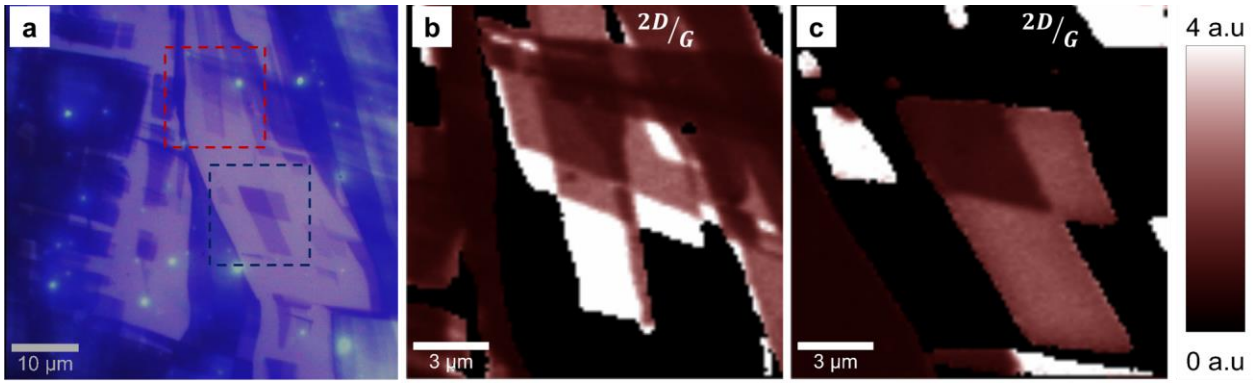

Fig. 1 (a) Optical micrograph of a sample region on a ~90 nm nanoparticle film with single and multi-layer flakes remaining after cleaving graphite from the surface. The red and blue box indicates the sample regions in (b) and (c), respectively, where Raman maps of the 2D/G peak intensity were taken with graphene having the highest intensity shown as white and graphite as maroon.

optically and then characterized by Raman microspectroscopy. Figure 1a shows a typical optical micrograph where a region of graphite was cleaved leaving single and multi-layer flakes on the surface. The bright "speckles" were found to be large nanoparticle aggregates that formed occasionally during the spin coating of the particle films. Figure 1b and 1c are Raman maps showing the ratio of the 2D/G bands of the sample regions selected (the red region in Figure 1b and the blue in Figure 1c) showing graphene as white with the highest intensity ratio, which decreases with increasing thickness up to bulk graphite seen as maroon. These maps were then used to identify specific regions where the samples could be further characterized and studied using Atomic Force Microscopy (AFM).

Surface Structure of the Graphene Films

The general morphology of the deposited graphene films were investigated first using AFM in both tapping and contact mode. The tapping mode topographic image in Figure 2a shows graphene lying over the crests of the rough surface with the underlying surface structure still visible due to the flexible nature of the graphene and its partial conformity to the substrate. The degree of conformity can be seen in the line profile in Figure 2b which reveals that for these surfaces the film is partially suspended over the surface asperities, as evident by the decreased height of the amplitude (down to *ca*. 1 nm) along the line profile. This behavior is very different from flat surfaces where graphene has been observed to fully conform to even atomic scale roughness.[37, 38] Some small wrinkles seen along the graphene edges were found to originate from intermittent contact with the AFM tip during scanning, likely due to the relatively weak adhesion and decreased contact with the substrate. Here the tip was able to lift up and partially drag the edges of the graphene flake. Under optimized imaging parameters, this wrinkling effect could be minimized, moreover it was rarely observed to occur during contact mode imaging, implying that a brief contact and lifting motion is required to slide the graphene over the rough surface. Although graphene exhibits high out-of-plane flexibility for conforming to surfaces of different geometries, the van der Waals adhesion forces in this case are clearly not large enough to overcome the inherent in-plane lattice strain imposed by the random distribution of nanoparticle crests on the surface to allow for a fully conformed state to be stabilized.

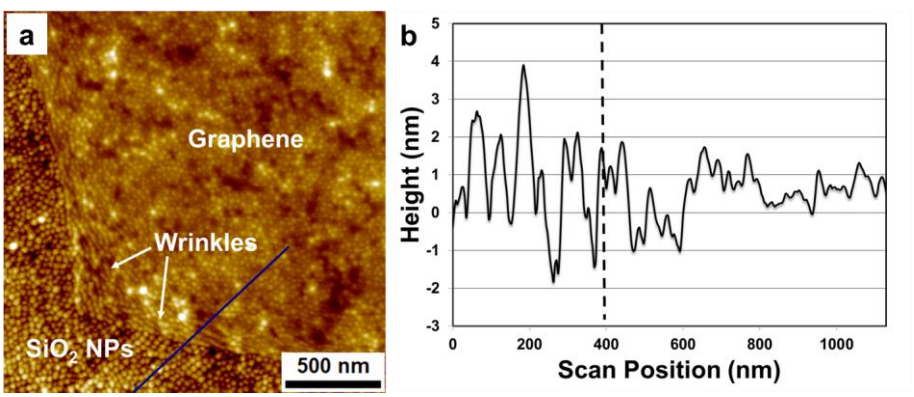

Fig. 2 (a) Tapping mode AFM topography image of a graphene flake on a rough silica nanoparticle substrate. (b) Line profile from the blue line in (a) showing the partial conformity of the graphene flake to the rough surface due to weak interfacial adhesion. The dashed line indicates the transition from the substrate to the graphene in the line profile.

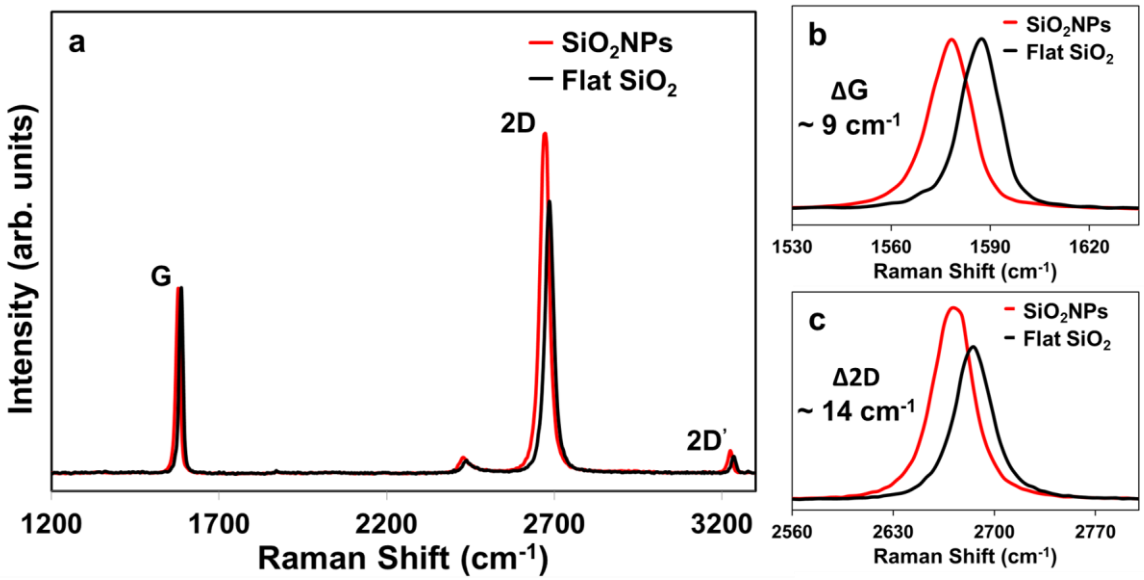

Fig. 3 (a) Raman spectra of graphene on a rough silica substrate compared to a flat silica surface showing the shift to lower wavenumber on a rough surface due to strain in the graphene lattice. (b) and (c) are larger views of the G and 2D peak shifts. The Raman spectra were normalized to the intensity of the G peak.

Raman Spectral Mapping of Graphene Strain

Raman microspectroscopy was used to confirm the presence of lattice strain as a critical factor in the resulting morphology of graphene on these rough surfaces. Raman is known to be sensitive for measuring the strain due to the changes in the crystal lattice, which alters the phonon frequencies.[39] To analyze the strain in the graphene induced by the rough substrate, graphene flakes were also exfoliated onto thermally grown SiO_2 on a Si(100) wafer using the same water soluble tape method as a reference sample. A comparison between the Raman spectra from both flat and rough unfunctionalized samples can be seen in Figure 3a. On the rough surface the characteristic G and 2D peaks show a clear shift to lower frequencies. The relative peak positions and widths were obtained by using a Lorentz fitting: on the flat surface the 2D and G bands appeared at ~ 2685 cm^{-1} (FWHM 30 cm^{-1}) and ~ 1587 cm^{-1} (FWHM 13 cm^{-1}) respectively, while on the rough surface the 2D band was observed at~ 2671 cm^{-1} (FWHM 31 cm^{-1}) and G at ~ 1578 cm^{-1} (FWHM 14 cm^{-1}). This yields approximately a 9 cm^{-1} G peak shift (Figure 3b) and a 14 cm^{-1} 2D peak shift (Figure 3c) between the two. A slight decrease in the 2D/G ratio was also observed indicating the graphene on the flat SiO_2 surface may be slightly more chemically doped, likely due to the increased contact with the substrate.[39] The larger shift in the 2D peak position however, indicates that the shift is dominated by strain instead of chemical doping and is very consistent with prior studies on biaxial strain in graphene.[39-43]

Effect of Thickness and Applied Load on Graphene-Substrate Conformity

Upon examining multi-layered graphene regions, the conformity to the substrate was found to decrease with increasing number of layers or thickness. This can be seen in Figure 4 as an obvious reduction in the roughness in the topographic image corresponding to a reduction in the visibility of the nanoparticle film structures. Once the thickness becomes large enough, the morphology appears to be identical to bulk graphite lying flat (rms roughness < 1 nm) over the rough substrate. It should also be noted that the decreasing conformity with increasing number of layers appears to proceed in gradual steps rather than a sharp "snap-through" transition which has been observed on larger corrugated structures.[44] However, the gradual transition can be similarly understood to be due to the increased bending stiffness of the structures with more layers.

The measured roughness and surface morphology of the graphene layers were expected to greatly depend on the imaging load,[45] which increased both the out-of-plane bending and in-plane stretching of the graphene lattice. Using AFM probes with tip radii of ~ 20 nm, the graphene showed increased conformity to the underlying substrate with increased load (Figure 5). This

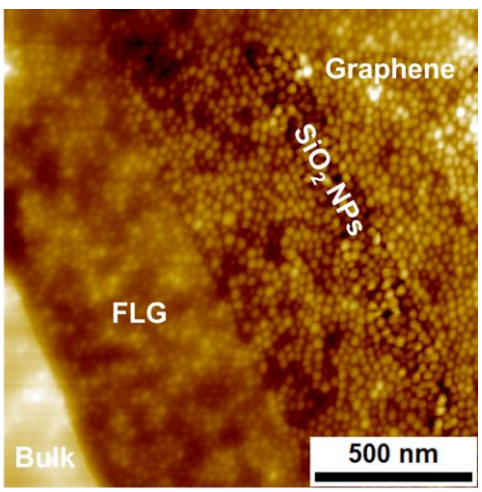

Fig. 4 Contact mode AFM topography image of the rough silica substrate and graphene layers with different thicknesses and bulk graphite. As the number of layers increased the underlying nanoparticle surface features become less visible due to the increasing stiffness in the layers.

change was measured by comparing the calculated roughness and surface area ratio (ratio of the measured interfacial surface area to the area of the projected x-y plane) as a function of normal load. Plotted in this way, the expected range of values start at zero for a flat surface and would maximize at the value measured for a typical rough surface (dashed line), which should be load independent, assuming no wear of the AFM tip. Two cases are shown for comparison: graphene and 3-layer graphene). It can be seen that, for the single-layer case, the roughness increased up to ~ 100 nN of normal tip load and then plateaued around 6.5 nm roughness where the graphene appeared to reach its maximum conformity for this tip size. Beyond 100 nN, the graphene lattice was further stretched and strained as indicated by the continued increase of the surface area ratio. In the case of 3-layers, there was initially some small roughness, which steadily increased with load, but was expectedly lower than the single-layer case due to the added thickness and increased bending stiffness.

Figure 6a and 6b show topographic images of single-layer graphene at 5 nN and 125 nN imaging load, while Figure 6d and 6e shows the topographic images of 3-layer graphene at the same loads. As can be readily seen by eye, the images at higher load appear sharper as the graphene films are compressed onto the substrate. Comparison of the line profiles in Figure 6c and 6f reveal that the graphene and 3-layer graphene regions are stretched by *ca.* 2 nm – 3 nm and 1 nm – 2 nm, respectively. Even at 125 nN the graphene was unable to fully conform to the surface in comparison to the typical values of ~ 9.5 nm roughness and 2.8% surface area ratio for the unmodified rough silica surface. This implies that even with increased energy from the mechanical tip loading, a fully conformed state was unable to be achieved due to the sharpness of the nanoparticle crests and the elastic restoring energy of graphene to reversibly deform, maintaining minimal strain energy at equilibrium. Using a relatively simplistic Hertz model[46-48] for the out-of-plane modulus comparing the displacement of the graphene in between the particles at low (5 nN) and high (125 nN) loads, one can estimate the out-of-plane modulus as a simple indentation. Using

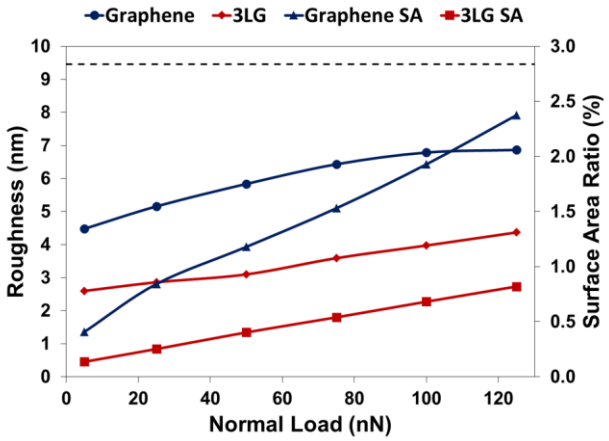

Fig. 5 RMS Roughness and surface area (SA) ratio as a function of normal load averaged over 1μm² scans for graphene and 3-layer graphene (3LG). The dashed line indicates the values for a bare silica nanoparticle surface independent of tip load. Error bars associated with these measurements are smaller than the symbols in the figure.

this model we estimate a modulus of *ca.* ~1 GPa. This estimate however is of course severely compromised by the fact that as the imaging load is increased, the contact is systematically changing from a tip on graphene which limited contact to the substrate to one where the tip-graphene-substrate contact area increases with increasing load. As such a uniaxial load on the center of the graphene by the AFM tip cannot be fully assumed.

The Frictional Properties

Again as real MEMS devices typically exhibit nanoscale roughness of *ca.* 10 nm, the ability of materials to modify the friction of rough surfaces must also be investigated. As such, friction force microscopy was used to evaluate the tribological

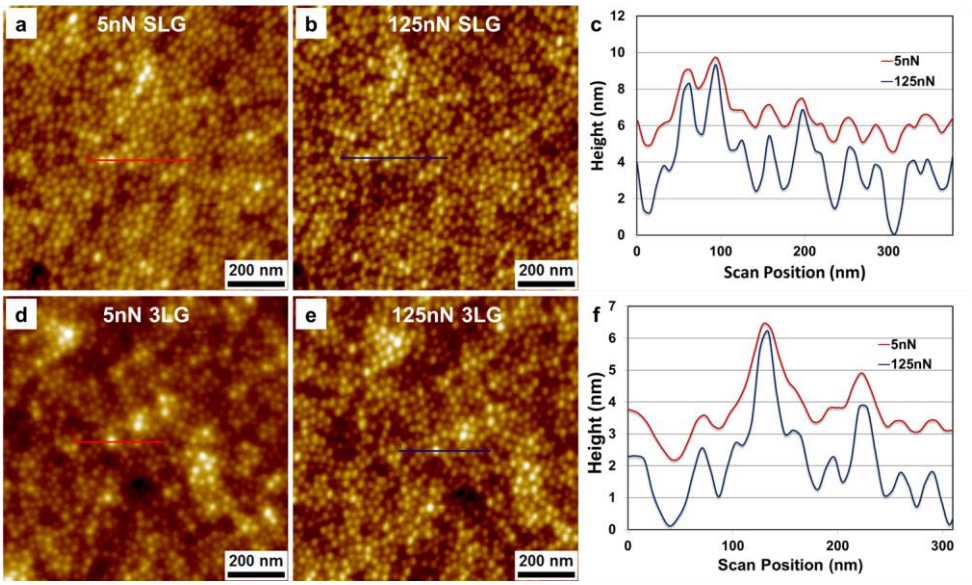

Fig. 6 Contact mode AFM topography images of graphene at 5 nN (a) and 125 nN (b) and the line profiles (c) from the red and blue lines in (a) and (b). Contact mode AFM topography images of 3-layer graphene (3LG) at 5 nN (d) and 125 nN (e) and the line profiles (f) from the red and blue lines in (d) and (e). The line profiles have been corrected for drift and are offset for easier comparison of the conformity and stretching behaviour of the graphene layers under different tip loads.

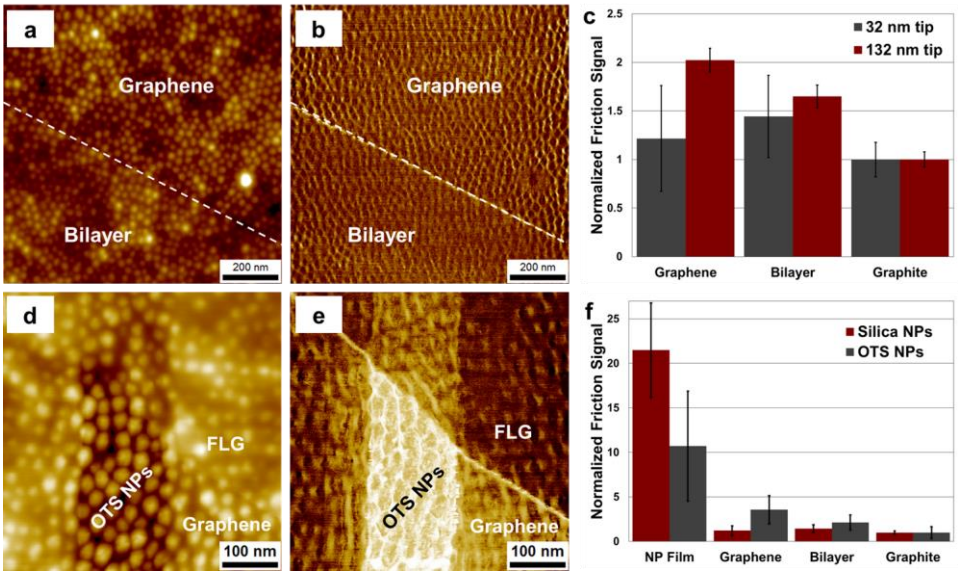

Fig. 7 Contact mode AFM topography images obtained with a sharp probe (a,d) and friction maps (b,e) of a sample region containing graphene layers on silica and OTS modified nanoparticles, respectively, for comparison of local roughness and friction. (c) Friction values of graphene layers using an AFM probe with a radius of 32 ± 2 nm and friction values of graphene layers using a blunter probe with a radius of 132 ± 17 nm. The friction and roughness values are normalized to that of bulk graphite to show the recovery of the friction trend with a larger AFM probe. (f) Normalized friction values of silica and OTS nanoparticles and graphene layers using an AFM probe with a radius of 32 ± 2 nm. The OTS coated nanoparticles show the typical "puckering effect" with reduced friction combined with graphene, but the overall friction is higher than the graphene on the unfunctionalized surface where the puckering effect is suppressed.

properties of graphene on these same surfaces. The topography comparing single and bi-layer graphene and the corresponding friction map is shown in Figure 7a and 7b, respectively. A small variation in roughness can be seen in the topography while no decrease in friction was observed with increasing number of layers. To compare the friction on different regions of the surface, the relative friction signal was averaged from individual friction maps and normalized to the value for bulk graphite, as determined *in situ* from measurements on graphitic flakes (> 5 layers) on the surface. The variation in friction with the number of layers however, was noticeably dependent upon the dimensions of the AFM tip. Figure 7c shows the normalized friction values comparing single-layer graphene, bi-layer graphene and graphite collected with both a sharp and blunt AFM tip. It was seen that with a sharp probe (radius of curvature of 32 nm ± 2 nm) there was not a significant change in friction between single graphene layers up to bulk-like graphite. Although the bi-layer appears to have slightly higher friction than graphene, this is within the error bars which are larger on rough surfaces due to the increased lateral bending of the cantilever (more so with a sharp probe) and generally larger noise associated with the friction measurements on rough surfaces. Further evaluation of the local roughness of the random sample regions taken for average measurements showed the bilayer had a slightly higher roughness at the low load of 5 nN thus increasing the friction. The result in Figure 7c was unexpected since the graphene is weakly adhered and has decreased contact to the surface but seemingly does not exhibit the characteristic "puckering effect" as observed on similarly fabricated flat substrate samples (see Supporting Information Figures S1-S2). While high resolution stick-slip images would normally be used to also examine if puckering was occurring, these could not be obtained on these rough graphene surfaces. Adhesion force mapping measurements were also conducted and showed little to no variance in measured adhesion as a function of the number of layers (Figure S3) indicative that puckering, which on a rough surface we would expect to express itself as layer dependent adhesion, was not occurring.

In contrast to the sharp probe, when a blunted silica probe (132 nm ± 17 nm) with a radius of curvature much greater than that of the surface asperities (~10 nm) of the underlying substrate was used, the friction of single-layer graphene was found to be 50% higher than the bulk and 20% higher than bi-layer, consistent with previous reported values on flat surfaces.[13, 23]

Not surprisingly, these findings indicate that the frictional properties of graphene on such rough surfaces depend strongly on the combined, effective contact area of the sliding interface. When the AFM tip radius is smaller, the total asperity-asperity contact is also smaller and changes smoothly as the tip moves laterally over the nanoparticle asperities. This prevents the graphene from being able to slide over the surface as easily as on flat surfaces, thus suppressing puckering in front of the tip. The larger, blunter probe simply has a larger contact area thus affording greater adhesion to the probe than to the substrate. The resulting increased shear stress can then induce sliding of the graphene, despite the roughness, and increase the measured friction. This suggests that for rough surfaces, a critical contact area dependence exists which balances the surface forces needed to mitigate this effect and afford good friction modification. One could imagine a blunt enough probe that would allow for multiple asperities to be contacted simultaneously which would balance out the tip-graphene contact area again resulting in the loss of any observed layer dependence, but this would depend on the relative distance between surface asperities as well, and will be the subject of future studies.

Influence of Hydrophobic Surface Interactions

As control of the graphene substrate contact significantly influences the observed friction, in addition to studying graphene

on hydrophilic substrates, hydrophobic substrates were also explored to investigate the influence of surface chemistry on the morphology and tribological properties of the deposited graphene. Here the silica nanoparticle films were functionalized with octadecyltrichlorosilane (OTS) and characterized with infrared spectroscopy (Figure S4). OTS coatings have been previously shown to reduce chemical doping of graphene from the substrate in field effect transistors and it can also provide additional pathways interfacial lubrication.[49, 50] Contact AFM imaging showed that the various graphene layers conform similarly to the OTS coated substrates as they did to the unfunctionalized supports (Figure S5a), with a similarly observed decrease in roughness with increasing layer thickness (Figure S5b). As with the unmodified substrates, only partial conformity was observed also due to strain from the rough substrate which was greater than the added interfacial adhesion. As the surface geometries are nominally the same (with an increase in surface asperities size of at most 10 % due to the added monolayer) the magnitude of the strain was expected to be nearly the same in both hydrophilic and hydrophobic samples. This was confirmed by the observation of similar G (6 cm^{-1}) and 2D (15 cm^{-1}) band peak shifts in the Raman spectra (Figure S6). The peak positions for graphene exfoliated onto the thermally grown oxide of a flat Si(100) wafer modified with OTS (2D ~ 2689 cm^{-1}, G ~ 1582 cm^{-1}) were also consistent with values for unstrained, undoped graphene (2D ~ 2692 cm^{-1}, G ~ 1582 cm^{-1}) indicating there was very little chemical doping effect from the substrate.[39] In comparison, a slight decrease in the 2D/G intensity was noted for graphene on the OTS modified nanoparticle surface, likely due to the increased disorder in the monolayer on these rough surfaces[51, 52] which results in more collapsed films, yielding slightly decreased buffering from substrate doping.

The largest effect of the functionalized surface was observed in the frictional properties. A significant contrast between the OTS modified nanoparticles, graphene and few-layer graphene can be easily seen in the AFM contact mode topographic image in Figure 7d and friction map in Figure 7e. The averaged friction signal showed that graphene had lower friction than OTS, but higher friction than bi-layer and bulk graphite on the substrate (Figure 7f). These results are also consistent with comparative flat OTS substrate studies, which also showed a very distinct "puckering effect" (Figures S7-S8). In this case, the friction was not found to depend on the contact area since the puckering effect was observed even with a sharp probe resulting in overall increased friction as compared to graphene layers on the unfunctionalized rough surface. This can be attributed to the slightly larger size of the nanoparticles and increased interfacial lubrication by the OTS film, which reduces the graphene-substrate friction allowing for easier sliding over the surface since the graphene is not strongly bound to the substrate.

Conclusions

AFM analysis of graphene on surfaces with nanoscale roughness showed that a tightly conformed state was not possible due to the large strain that would be required, leaving graphene weakly adhered at the peaks of the substrate asperities and only partially conformed to the underlying substrate morphology. Conformity to the substrate was also found to decrease with increasing number of graphene layers, but it could be increased under higher applied mechanical loads during imaging, elastically returning to a less conformed state with decreased imaging load. The frictional properties were found to depend on the relative adhesion between the AFM probe tip and the substrate, with suppression of the "puckering effect" under asperity-asperity contact due to the large surface roughness and low adhesion to the tip. With a larger AFM tip which is able to contact multiple asperities at any given time, increased friction on graphene from the increased contact area and shear was observed. Substrate chemistry was also found to modulate the interactions and measured friction, as graphene on hydrophobic OTS functionalized substrates showed a strong affinity for the substrate, but with higher friction for single-layer graphene as compared to multiple layers, and higher friction as compared to graphene on the hydrophilic silica substrate. This increased friction may in part be due to increased shear strain brought about by the more compliant OTS layer under the graphene as compared to the bare silica support. These findings contribute to the understanding of graphene-substrate interactions by examining the balance between substrate geometry, surface chemistry, graphene bending energy, and lattice strain. They point to an optimal configuration for controlling friction by tailoring of self-assembled monolayers as a buffer layer that can provide additional pathways for energy dissipation in contacts, control over the surface energy and increased binding to rough surfaces. Additionally, utilizing silica surfaces with controlled roughness may provide a platform for using strain as a way to further modulate the electronic properties of graphene and as a means to control the extent of substrate chemical doping effects.

Acknowledgements

We gratefully acknowledge support for this research from the US National Science Foundation under grants CMMI -1131361, CMMI-1436192 and CHE-1062840.

1. K. S. Novoselov, A. K. Geim, S. V. Morozov, D. Jiang, Y. Zhang, S. V. Dubonos, I. V. Grigorieva and A. A. Firsov, *Science*, 2004, **306**, 666-669.
2. X. Du, I. Skachko, A. Barker and E. Y. Andrei, *Nat Nano*, 2008, **3**, 491-495.
3. A. A. Balandin, S. Ghosh, W. Bao, I. Calizo, D. Teweldebrhan, F. Miao and C. N. Lau, *Nano Letters*, 2008, **8**, 902-907.
4. C. Lee, X. Wei, J. W. Kysar and J. Hone, *Science*, 2008, **321**, 385-388.
5. K.-S. Kim, H.-J. Lee, C. Lee, S.-K. Lee, H. Jang, J.-H. Ahn, J.-H. Kim and H.-J. Lee, *ACS Nano*, 2011, **5**, 5107-5114.
6. F. Wählisch, J. Hoth, C. Held, T. Seyller and R. Bennewitz, *Wear*, 2013, **300**, 78-81.
7. A. L. Kitt, Z. Qi, S. Rémi, H. S. Park, A. K. Swan and B. B. Goldberg, *Nano Letters*, 2013, **13**, 2605-2610.
8. S. Stankovich, D. A. Dikin, G. H. B. Dommett, K. M. Kohlhaas, E. J. Zimney, E. A. Stach, R. D. Piner, S. T. Nguyen and R. S. Ruoff, *Nature*, 2006, **442**, 282-286.
9. Z. Chen, S. Berciaud, C. Nuckolls, T. F. Heinz and L. E. Brus, *ACS Nano*, 2010, **4**, 2964-2968.
10. M. D. Stoller, S. Park, Y. Zhu, J. An and R. S. Ruoff, *Nano Letters*, 2008, **8**, 3498-3502.
11. F. Xia, D. B. Farmer, Y.-m. Lin and P. Avouris, *Nano Letters*, 2010, **10**, 715-718.
12. J. S. Bunch, A. M. van der Zande, S. S. Verbridge, I. W. Frank, D. M. Tanenbaum, J. M. Parpia, H. G. Craighead and P. L. McEuen, *Science*, 2007, **315**, 490-493.
13. C. Lee, Q. Li, W. Kalb, X.-Z. Liu, H. Berger, R. W. Carpick and J. Hone, *Science*, 2010, **328**, 76-80.
14. J. H. Seol, I. Jo, A. L. Moore, L. Lindsay, Z. H. Aitken, M. T. Pettes, X. Li, Z. Yao, R. Huang, D. Broido, N. Mingo, R. S. Ruoff and L. Shi, *Science*, 2010, **328**, 213-216.
15. W. Cai, A. L. Moore, Y. Zhu, X. Li, S. Chen, L. Shi and R. S. Ruoff, *Nano Letters*, 2010, **10**, 1645-1651.
16. J.-K. Lee, S. Yamazaki, H. Yun, J. Park, G. P. Kennedy, G.-T. Kim, O. Pietzsch, R. Wiesendanger, S. Lee, S. Hong, U. Dettlaff-Weglikowska and S. Roth, *Nano Letters*, 2013, **13**, 3494-3500.

17. T. Kase and T. Ogino, *The Journal of Physical Chemistry C*, 2013, **117**, 15991-15995.
18. Q. Wu, Y. Wu, Y. Hao, J. Geng, M. Charlton, S. Chen, Y. Ren, H. Ji, H. Li, D. W. Boukhvalov, R. D. Piner, C. W. Bielawski and R. S. Ruoff, *Chemical Communications*, 2013, **49**, 677-679.
19. W. Zhu, T. Low, V. Perebeinos, A. A. Bol, Y. Zhu, H. Yan, J. Tersoff and P. Avouris, *Nano Letters*, 2012, **12**, 3431-3436.
20. S. J. Goncher, L. Zhao, A. N. Pasupathy and G. W. Flynn, *Nano Letters*, 2013, **13**, 1386-1392.
21. S. p. Berciaud, S. Ryu, L. E. Brus and T. F. Heinz, *Nano Letters*, 2008, **9**, 346-352.
22. Z. Luo, Y. Lu, D. W. Singer, M. E. Berck, L. A. Somers, B. R. Goldsmith and A. T. C. Johnson, *Chemistry of Materials*, 2011, **23**, 1441-1447.
23. D.-H. Cho, L. Wang, J.-S. Kim, G.-H. Lee, E. S. Kim, S. Lee, S. Y. Lee, J. Hone and C. Lee, *Nanoscale*, 2013, **5**, 3063-3069.
24. R. Maboudian and C. Carraro, *Annual Review of Physical Chemistry*, 2004, **55**, 35-54.
25. C. Hao, Y. Yin and C. Shaohua, *Journal of Physics D: Applied Physics*, 2013, **46**, 205303.
26. G. Wei and H. Rui, *Journal of Physics D: Applied Physics*, 2011, **44**, 452001.
27. Z. H. Aitken and R. Huang, *Journal of Applied Physics*, 2010, **107**, 123531-123510.
28. S. Scharfenberg, N. Mansukhani, C. Chialvo, R. L. Weaver and N. Mason, *Applied Physics Letters*, 2012, **100**, 021910-021913.
29. J. Zhang, Y. Wang and X. Wang, *Nanoscale*, 2013, **5**, 11598-11603.
30. T. J. W. Wagner and D. Vella, *Applied Physics Letters*, 2012, **100**, 233111-233114.
31. T. Li and Z. Zhang, *Nanoscale Research Letters*, 2009, **5**, 169-173.
32. A. Reserbat-Plantey, D. Kalita, Z. Han, L. Ferlazzo, S. Autier-Laurent, K. Komatsu, C. Li, R. Weil, A. Ralko, L. Marty, S. Guéron, N. Bendiab, H. Bouchiat and V. Bouchiat, *Nano Letters*, 2014, **14**, 5044-5051.
33. J. H. Prosser, T. Brugarolas, S. Lee, A. J. Nolte and D. Lee, *Nano Letters*, 2012, **12**, 5287-5291.
34. K. T. Cook, K. E. Tettey, R. M. Bunch, D. Lee and A. J. Nolte, *ACS Applied Materials & Interfaces*, 2012, **4**, 6426-6431.
35. J. E. Sader, J. W. M. Chon and P. Mulvaney, *Review of Scientific Instruments*, 1999, **70**, 3967-3969.
36. J. Batteas, X. Quan and M. Weldon, *Tribol Lett*, 1999, **7**, 121-128.
37. M. Ishigami, J. H. Chen, W. G. Cullen, M. S. Fuhrer and E. D. Williams, *Nano Letters*, 2007, **7**, 1643-1648.
38. W. G. Cullen, M. Yamamoto, K. M. Burson, J. H. Chen, C. Jang, L. Li, M. S. Fuhrer and E. D. Williams, *Physical Review Letters*, 2010, **105**, 215504.
39. J. Zabel, R. R. Nair, A. Ott, T. Georgiou, A. K. Geim, K. S. Novoselov and C. Casiraghi, *Nano Letters*, 2011, **12**, 617-621.
40. C. Metzger, S. Rémi, M. Liu, S. V. Kusminskiy, A. H. Castro Neto, A. K. Swan and B. B. Goldberg, *Nano Letters*, 2009, **10**, 6-10.
41. F. Ding, H. Ji, Y. Chen, A. Herklotz, K. Dörr, Y. Mei, A. Rastelli and O. G. Schmidt, *Nano Letters*, 2010, **10**, 3453-3458.
42. W. Pan, J. Xiao, J. Zhu, C. Yu, G. Zhang, Z. Ni, K. Watanabe, T. Taniguchi, Y. Shi and X. Wang, *Sci. Rep.*, 2012, **2**.
43. Y. Zhao, X. Liu, D. Y. Lei and Y. Chai, *Nanoscale*, 2014, **6**, 1311-1317.
44. S. Scharfenberg, D. Z. Rocklin, C. Chialvo, R. L. Weaver, P. M. Goldbart and N. Mason, *Applied Physics Letters*, 2011, **98**, 091908-091903.
45. Z. Osvath, E. Gergely-Fulop, N. Nagy, A. Deak, P. Nemes-Incze, X. Jin, C. Hwang and L. P. Biro, *Nanoscale*, 2014, **6**, 6030-6036.
46. B. N. J. Persson, *Surface Science Reports*, 2006, **61**, 201-227.
47. U. D. Schwarz, *Journal of Colloid and Interface Science*, 2003, **261**, 99-106.
48. J. Martín, M. Muñoz, M. Encinar, M. Calleja and M. Martín-González, *Langmuir*, 2014, **30**, 5217-5223.
49. M. Lafkioti, B. Krauss, T. Lohmann, U. Zschieschang, H. Klauk, K. v. Klitzing and J. H. Smet, *Nano Letters*, 2010, **10**, 1149-1153.
50. J. Ou, Y. Wang, J. Wang, S. Liu, Z. Li and S. Yang, *The Journal of Physical Chemistry C*, 2011, **115**, 10080-10086.
51. B. W. Ewers and J. D. Batteas, *The Journal of Physical Chemistry C*, 2012, **116**, 25165-25177.
52. R. L. Jones, N. C. Pearsall and J. D. Batteas, *The Journal of Physical Chemistry C*, 2009, **113**, 4507-4514.

